Mohamed et al. 2014. *Int. J. Vehicle Structures & Systems*, 6(1-2), 8-16
ISSN: 0975-3060 (Print), 0975-3540 (Online)
doi: 10.4273/ijvss.6.1-2.02

International Journal of Vehicle Structures & Systems
Available online at www.maftree.org/eja

Analysis and Testing for Slip Characteristics of Artificial Hydraulic Circuit based Push-Belt Continuously Variable Transmission

Eid S. Mohamed[a] and Saeed A. Albatlan[b]

[a]*Automotive and Tractors Engg.,*
Helwan University, Mataria, Cairo, Egypt.
Corresponding Author, Email: eng_eid74@yahoo.com

[b]*Automotive Engg., Higher Technological Institute, 6th of October City Campus, Egypt.*
Email: saeedzeed@yahoo.com

ABSTRACT:

Applying a Continuously Variable Transmission (CVT) in an automotive driveline has several advantages. A CVT can operate at a wider range of transmission ratios, therefore the engine can be operated more efficiently than with a stepped transmission. The present research focuses on the influence of loading conditions on the slip behaviour and torque transmission of the CVT. The CVT model is developed to investigate the range of clamping forces needed to initiate the transmission and to successfully meet the oil pressure requirements. An analytical approach is used to calculate the possible transmission efficiency and traction coefficient of the push belt CVT. The experimental setup and the instrumentation are presented in detail. The measured results are presented in more detail for the V-belt type variator and oil pressure reapplication by a separate hydraulic unit and reduction ratio of CVT.

KEYWORDS:

Continuously variable transmission; Metal-push belt; Slip characteristics; Clamping force; Modelling

CITATION:

E.S. Mohamed and S.A. Albatlan. 2014. Analysis and Testing for Slip Characteristics of Artificial Hydraulic Circuit based Push-Belt Continuously Variable Transmission, *Int. J. Vehicle Structures & Systems*, 6(1-2), 8-16. doi:10.4273/ijvss.6.1-2.02

ACRONYMS & NOMENCLATURE:

DCV	*Directional Control Valve*
CVT	*Continuously Variable Transmission*
CV	*Choke Valve*
RMS	*Root Mean Square*
T	*The band tension (N)*
F_1	*Inertia force (N)*
T_1, T_2	*Belt tension at ends of the element (N)*
F_c	*Centrifugal force (N)*
F_F	*Friction force acting between band pack and segment or between neighbouring bands (N)*
F_N	*Normal force acting on the segment shoulder (N)*
F_T	*Tangential friction force acting between the pulley surface and the segment side (N)*
F_R	*Radial friction force acting between the pulley surface and the segment sides (N)*
F_{axle}	*Axial force acting on the segment (N)*
m	*Mass of one belt segment (kg)*
V	*The velocity of the segment (m/s)*
R	*The rolling radius of the belt segment (m)*
d_{sec}, R_{sec}	*Diameter, Radius of the secondary pulley (m)*
d_{pri}, R_{pri}	*Diameter, Radius of the primary pulley (m)*
C	*Center distance (m)*
β_{pri}	*Contact angle for primary pulley (deg)*
β_{sec}	*Contact angle for secondary pulley (deg)*
i_{cvt}	*Transmission ratio of CVT*
L	*Belt length (m)*
P_p, P_s	*Primary & secondary oil pressure (N/m^2)*
A_p, A_s	*Primary & secondary piston area (m^2)*
ω_p, ω_s	*Primary & secondary pulley velocity (rpm)*
x_p, x_s	*Distance of the primary & secondary pistons (m)*
Δx	*Initial distance of secondary pulley spring (m)*
F_{spr}	*Force of secondary pulley spring (N)*
C_p, C_s	*Primary & secondary pulleys centrifugal coefficient*
μ_p, μ_s	*Primary & secondary pulley and belt traction coeff.*

1. Introduction

Continuously Variable Transmission (CVT) is increasingly used in automotive applications. It has an advantage over conventional automatic transmissions, with respect to the large transmission ratio coverage and absence of comfort issues related to shifting events. For this reason, CVT equipped cars are more economical than the cars equipped with planetary gear automatic transmissions. The key advantages of a CVT are higher engine efficiency, higher fuel economy, smooth acceleration without shift shocks and infinite gear ratios with a small number of parts. Fig. 1 illustrates the basic arrangement of a metal V-belt CVT.

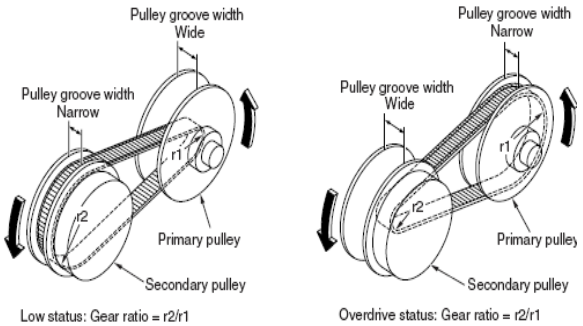

Fig. 1: System pulley arrangement

The basic configuration of a metal V-belt CVT consists of two variable diameter pulleys connected by a power-transmitting device, i.e. a metal V-belt. The pulley centers are at fixed distance apart. The pulley on the engine side is called the primary or driver pulley. The pulley on the wheel side is the secondary or driven pulley. Since one of the sheaves on each pulley is movable, the application of an axial force on the movable pulley sheave allows the belt to move radially in the pulley groove. The speed-ratio varies by changing the radial belt position towards the pulley center. In addition to the radial motion, the belt also moves tangentially around the pulley under the influence of an applied torque. The band pack runs over the belt elements, whereas the belt element contacts the band pack and pulley sheave. The metal V-belt is made of two series of thin steel bands holding together thin trapezoidal elements. The elements are connected to each other by a system of pegs and holes, a peg in the forward face of an element connected to a hole in the rear face of the element in front as shown in Fig. 2. Usually, an initial gap exists between the elements of the belt as they are not tightly pressed together [1].

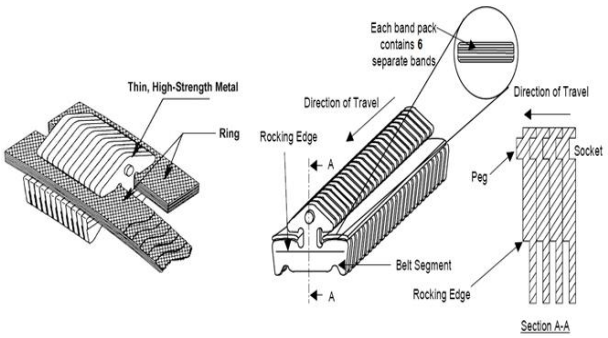

Fig. 2: Metal Push V-belt [3]

Dynamic modelling of CVT belts have been dealt by researchers in areas of load analysis and vibration modelling. An analytical modelling and experimental tests for obtaining the load distribution between bands is proposed. This model was composed of a multilayer belt without segments. The friction coefficient between layers should be slightly higher than that between inner layer and segments for a better distribution of forces between layers. In other work for push-belt by using a numerical model, forces in a CVT belts were obtained [2]. Braine [3] proposed a speed ratio-torque load-axial force relationship to calculate belt slip using the equations of motion under quasi-static equilibrium. The gross slip points depend on the torque transmission of the driven side. Numerical results showed that the belt radial displacement increased in the radial inward direction for driven pulley, while that of the driver pulley increased slightly and decreased with the increasing torque load. The effects of inertia and flexure were neglected and the band tension was assumed to be constant. Radial stiffness of belt was incorporated in order to analyze the influence of axial force on the radial penetration [3].

The focus is on the gap distribution between the elements and analysis of the mechanism causing micro-slip in a metal belt CVT. The authors also investigated the torque transmitting capacity of a metal V-belt CVT under no load conditions on driven pulley. The belt slip was calculated on the basis of mean gap. The slip ratio rises to a state of macro-slip when the transmitted torque exceeds the slip-limit torque. The slip was assumed to occur only on the pulley where the gaps were present and these elemental gaps were assumed to be distributed evenly in the idle sector at the entrance to the loading pulley [4].

Torque is transmitted from the driver to the driven pulley by the pushing action of the belt elements. Since there is friction between the bands and the elements, the bands also aid in torque transmission. So, there is a combined push-pull action in the belt that enables torque transmission. The torque capacity of metal belt CVTs under the conditions of quasi-static equilibrium and impending slip are investigated by Shiznu et al[5] and Bas et al[6], since the belt was assumed to be under the conditions of gross-slip, all the frictional forces were circumferentially directed. Only the inertial effects arising from centripetal acceleration were taken into account. It was proposed that the torque transmission capacity was limited by the maximum belt tension and the associated fatigue strength of the tension members. It was observed that for a given belt design, increasing the width with proportional changes in tension capability and mass led to a proportional increase in torque capacity. Optimization with respect to belt pitch radius yielded a 1-5 % increase in the torque capacity of the CVT system. This could be larger or smaller depending on the initial configuration of the drive [5, 6].

Carbore et al. [7] studied the influence of thermal effects on the performance and the life of a rubber V-belt drive by developing a simple heat transfer model based on conduction and convection effects. The heat is generated at the surface of the belt due to the sliding between the belt and the pulley. Heat is also generated inside the belt due to hysteresis. The author suggested that thermal effects due to hysteresis significantly influence the life of a belt drive and identified four major failure modes in rubber V-belts: cord rupture due to high torques, cord separation at moderate torques, radial cracks, and abrasion. Of these, cord separation mode was the most prevalent. It was attributed to the shear stresses occurring in the belt. Radial cracks start at the bottom of the belt and propagate towards the cord layer. They were attributed to the compressive stresses in the belt under low torque applications. The author also observed that abrasion was more prevalent in drives with locked-center distance than in drives with variable center distance.

The present research focuses on the influence of loading conditions on the slip behaviour and torque transmission of the CVT. The CVT model is developed to investigate the range of clamping forces needed to initiate the transmission and to successfully meet the oil pressure requirements. An analytical approach is used to calculate the possible transmission efficiency and traction coefficient of the push belt CVT. The experimental setup and the instrumentation are presented in detail. The measured results are presented in more detail for the V-belt type variator and oil pressure reapplication by a separate hydraulic unit and reduction ratio of CVT.

2. Belt geometry

The V-belt type variator appears in a few different forms depending upon the materials used in the belt or chain and the shape of the pulleys. The pulley set on the engine side of the transmission, is referred to as the primary pulley, the pulley set on the output shaft is called the secondary pulley. Each pulley consists of a fixed and a moveable pulley sheave [8].

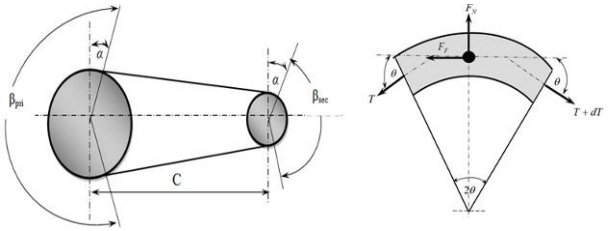

Fig. 3: Belt geometry

The primary and secondary moveable sheaves are on opposite sides of the belt, as shown in Fig. 3. Mostly only one part of the pulley moves and the axial position of the belt is not constant as,

$$L=\sqrt{4C^2-\left(d_{\sec}-d_{pri}\right)^2}+\frac{1}{2}\left(d_{pri}\beta_{pri}+d_{\sec}\beta_{\sec}\right) \tag{1}$$

Dividing Eqn. (1) by C gives,

$$\frac{L}{C}=\sqrt{4-\left(\frac{d_{\sec}-d_{pri}}{C}\right)^2}+\frac{1}{2C}\left(d_{pri}\beta_{pri}+d_{\sec}\beta_{\sec}\right) \tag{2}$$

Since the length of the belt, L, is known, the distance between pulley centres, C, can be calculated in iteratively to find corresponding values of primary and second pulley diameters d_{pri} and d_{sec} and β_{pri} and β_{sec} for any value of transmission ratio using,

$$i=\frac{d_{\sec}}{d_{pri}}= \tag{3}$$

$$\beta_{pri}=\pi-2\sin^{-1}\left(\frac{d_{\sec}-d_{pri}}{2C}\right)=\pi-2\sin^{-1}\left[0.5\frac{d_{pri}}{C}\left(i-1\right)\right] \tag{4}$$

$$\beta_{\sec}=\pi+2\sin^{-1}\left(\frac{d_{\sec}-d_{pri}}{2C}\right)=\pi+2\sin^{-1}\left[0.5\frac{d_{pri}}{C}\left(i-1\right)\right] \tag{5}$$

3. Metal push belt model

3.1. Relative velocity between CVT components

Fig. 4 shows the relative velocities between the band pack and pulley sheave. The segments will be travelling at a rolling radius of R_1 and R_2 about the pulleys, such that the linear velocity of each of the segments, v, may be calculated at loaded and no loaded conditions.

$$v=\omega_{pri}R_{pri}=\omega_{\sec}R_{\sec} \tag{6}$$

At no load condition, the spin point (s) is located close to the center (c) such that x=0 the velocity at no load conditions are derived as follows.

$$v=\omega_{pri}R_{pri}=\omega_{\sec}R_{\sec}$$

$$\omega_{pri}=\frac{R_{\sec}}{R_{pri}}\omega_{\sec}=i\omega_{\sec} \tag{7}$$

$$v_{pri(x)}=\left(R_{pri}+x\sin\alpha\right)=\omega_{pri}\Big|_{-b}^{+b}$$

$$v_{\sec(x)}=\left(R_{\sec}+x\sin\alpha\right)=\omega_{\sec}\Big|_{-b}^{+b}$$

$$v_{s(x)}=\left(R_{pri}+x\sin\alpha\right)=\omega_{pri}-\left(R_{\sec}+x\sin\alpha\right)\omega_{\sec}\Big|_{-b}^{+b} \tag{8}$$

The maximum and minimum values of velocities are,

$$v_{pri}\left(\max\right)=\left(R_{pri}+b\sin\alpha\right)\omega_{pri}$$

$$v_{\sec}\left(\max\right)=\left(R_{\sec}+b\sin\alpha\right)\omega_{\sec}$$

$$v_{pri}\left(\min\right)=\left(R_{pri}-b\sin\alpha\right)\omega_{pri}$$

$$v_{\sec}\left(\min\right)=\left(R_{\sec}-b\sin\alpha\right)\omega_{\sec}$$

$$V_S\left(\max\right)=v_{pri}\left(\max\right)-v_{\sec}\left(\max\right) \tag{9}$$

$$V_S\left(\min\right)=v_{pri}\left(\min\right)-v_{\sec}\left(\min\right) \tag{10}$$

At loaded conditions, the spin point (s) moves towards the open, such that x=-s and

$$\left(R_{pri}-s\sin\alpha\right)\omega_{pri}=\left(R_{\sec}-s\sin\alpha\right)\omega_{\sec}$$

$$i=\frac{\omega_{pri}}{\omega_{\sec}}=\frac{R_{\sec}-s\sin\alpha}{R_{pri}-s\sin\alpha} \tag{11}$$

$$V_S=\omega_{pri}\left[\left(R_{pri}+x\sin\alpha\right)-\frac{\left(R_{\sec}+x\sin\alpha\right)\left(R_{pri}-s\sin\alpha\right)}{\left(R_{\sec}-s\sin\alpha\right)}\right] \tag{12}$$

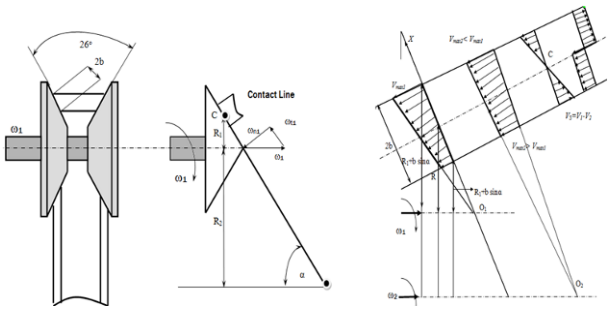

Fig. 4: Relative velocities between the band pack and pulley sheave

3.2. Kinetics of push belt CVT

The CVT system runs at constant transmission ratio. The driver and driven pulleys run at constant angular velocities and are subjected to loading conditions of torques and axial forces. The belt inertial effects have been neglected, except for the terms arising from the centripetal acceleration of the belt. Fig. 5 shows the geometry of the band pack around a number of belt segments while travelling around a pulley wrap angle.

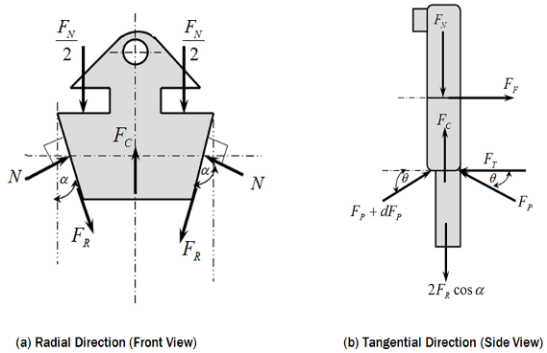

Fig. 5: Free body diagram of force acting in one segment

Tangential slip is modelled on the basis of gap redistribution between the belt elements. For the analysis of push V-belt, taking sum of forces in X, Y, tangential and radial directions [9, 10] respectively give:

$$(T+dT)\cos\theta = F_F + T\cos\theta \quad (13)$$

$$(T+dT)\sin\theta + T\sin\theta = F_N \quad (14)$$

$$F_T + F_P\cos\theta = F(F_P + dF_P)\cos\theta + F_F \quad (15)$$

$$F_N + 2F_R\cos\alpha = F_C + (2F_P + dF_P)\sin\theta + 2N\sin\alpha \quad (16)$$

Where $F_C = mv^2/R$. A substitution for the normal force acting on the segment side may be made to introduce the axial force acting on the segment as follows,

$$F_N + 2F_R = m\frac{v^2}{R} + (2F_P + dF_P)\frac{0.5t}{R} + 2F_{axle}\tan\alpha \quad (17)$$

$$F_R + F_C = (T+dT)^* d\theta + T^* d\theta \quad (18)$$

$$(T+dT)\cos d\theta + F_1 = T\cos d\theta + F_f \quad (19)$$

$$(T+dT)mr^2\gamma^* d\theta = T + F_N\mu$$

$$dT = \mu(T - mv^2) - mr^2\gamma^* d\theta \quad (20)$$

$$\int_{T2}^{T1}\frac{dT}{T - m^2 - \frac{(r^2)\gamma}{\mu}} = \int_0^{\theta}\mu d\theta$$

$$T_1 - T_2 = \left[T_1 - m\left(v^2 + r^2\frac{\gamma}{\mu}\right)\right]\left(1 - e^{-\mu\theta}\right) \quad (21)$$

3.3. Belt friction characteristics

The V-belt type CVT utilizes friction to transmit power from the primary pulley to the secondary pulley. Traction curve is the dimensionless relationship between transmitted torque and the slip. The maximum input torque that can be transmitted by the CVT is dependent on the applied clamping force. The belt slip speed and the belt friction coefficient increase when the transmission torque increase. The traction coefficient is therefore chosen to be a dimensionless value [11, 12]. The traction coefficient of primary and secondary side, μ_p and μ_s are defined as:

$$\mu_p = \frac{T_p\cos\alpha}{2F_pR_p} \text{ and } \mu_s = \frac{T_s\cos\alpha}{2F_sR_s} \quad (22)$$

Where T_p and T_s represent the input and output torque. R_p and R_s represent the primary and secondary running radius of the belt on the pulley. F_p and F_s represent the primary and secondary clamping forces and α is the pulley wedge angle. The transmission efficiency of the CVT (η_T) is given by the ratio of the output and the input power of the transmission:

$$\eta_T = \frac{P_{out}}{P_{inp}} = \frac{\omega_s T_s}{\omega_p T_p} \quad (23)$$

Power loss of the CVT from this equipment is given by,

$$P_{loss} = P_{inp} - P_{out} = \frac{2\pi(n_pT_p - n_sT_s)}{60000} \quad (24)$$

The power loss given by Eqn. (24) includes slipping losses arising between each contacting component in the CVT, the belt torque loss caused by the resistance to radial resistance and the loss from four bearings supporting the pulley shafts.

3.4. Dynamic model of CVT

The driveline model for the CVT is schematically depicted in Fig. 6. The model incorporates the motor inertia I_D, load inertia I_L, system primary and secondary damping (B_p, B_s) and stiffness (K_p, K_s) [13] using:

$$I_D\ddot{\theta}_D = B_p(\dot{\theta}_D - \dot{\theta}_P) + K_p(\theta_D - \theta_p) - F_pR_pK(t) \quad (25)$$

$$I_L\ddot{\theta}_L = -B_s(\dot{\theta}_s - \dot{\theta}_L) - K_s(\theta_s - \theta_L) + F_sR_sK(t) \quad (26)$$

Where $K(t) = F_p/F_s$

For primary side, $\dot{\theta}_p = \dot{\omega}_p$, $\dot{\theta}_p = \omega_p$

For secondary side, $\ddot{\theta}_s = \dot{\omega}_s$, $\dot{\theta}_s = \omega_s$

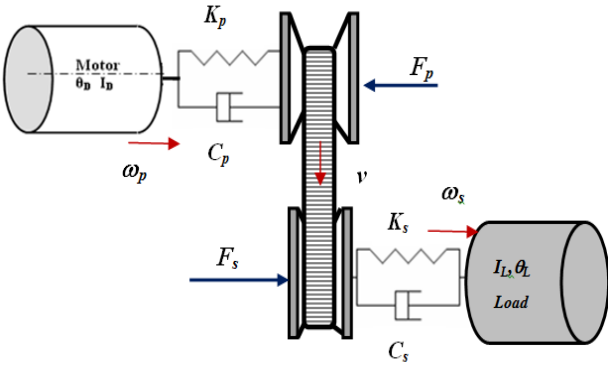

Fig. 6: Dynamic model of CVT

4. Simulation results and discussions

The simulations were conducted on MATLAB platform. The model required the input of design parameters. The characteristics of metal belt CVT that influence its response to the loading conditions were assessed through numerous simulations for different loading conditions in order to understand the dynamics of CVT under steady-state conditions. The impending motion in the model is such that the belt starts to move downwards in the driver pulley sheave and upwards in the driven pulley sheave. The transmission ratio for the model is defined as the ratio of belt pitch radius on driver pulley to belt pitch radius on driven pulley. Table 1 gives the parameter values used in the simulation [14].

Table 1: Main parameters of push belt CVT

Parameter	Symbol	Unit	Value
Pulley centre distance	C	m	0.26
Transmission ratio range	i_{cv}	--	2.5-0.8
Primary Max. input torque	T_i	Nm	400
Coefficient of friction	μ	---	0.15
Half pulley wedge angle	θ	deg.	13
Number of bands	i_p	---	6
Thickness of an individual band	t_{ban}	m	$2.1*10^{-4}$
Thickness of segment	t_{seg}	m	$5.5*10^{-3}$
Secondary spring stiffness	K_s	N/m	$10.2*10^3$

Fig. 7 shows the calculated belt radii about each pulley for the complete range of transmission ratios. An 'overdrive' condition is described by i_{cvt} <1. Fig. 8 shows the tensile force profiles for the band pack on the driver

and driven pulleys. The band tensile force decreases from the inlet to the exit of the driver pulley, whereas, it increases from the inlet to the exit of the driven pulley. Fig. 9 illustrates angles of wrap about each pulley. The simulation is undertaken with constant input speed of 1600 rpm and torque of 120 Nm. The elements pack up as the belt moves around the pulleys, and consequently the compressive force in the belt increases.

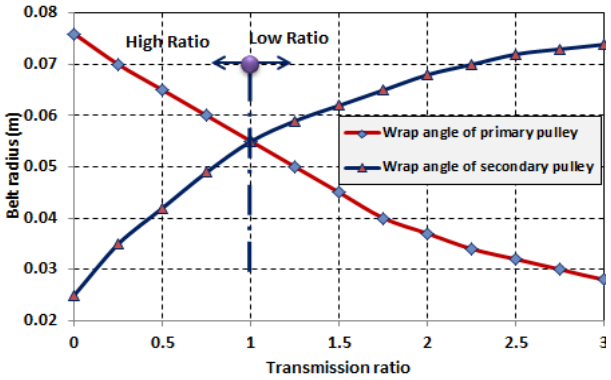

Fig. 7: Belt Radius vs. Transmission ratio

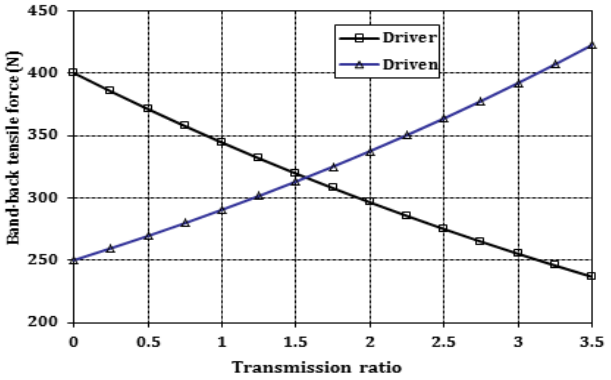

Fig. 8: Band pack tensile force on the driver and driven pulleys

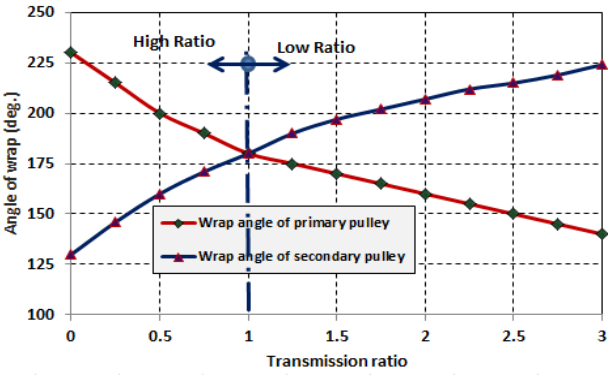

Fig. 9: Variator wrap angle vs. Transmission ratio

Fig. 10 illustrates the transmission torque variation with transmission ratio at different values of clamping force 1000 and 8000N. High value of clamping force results an increase in the transmission torque. The model is able to sustain lower load torque conditions at higher transmission ratios than at lower transmission ratios. For Fig. 11 illustrates the variation of the traction coefficient with primary input speed 800, 1600 and 3000 rpm conditions for different slip ratios. Fig. 12 illustrates the variation of the traction coefficient with CVT transmission ratios 0.8, 1, and 2.6 conditions for different slip ratios.

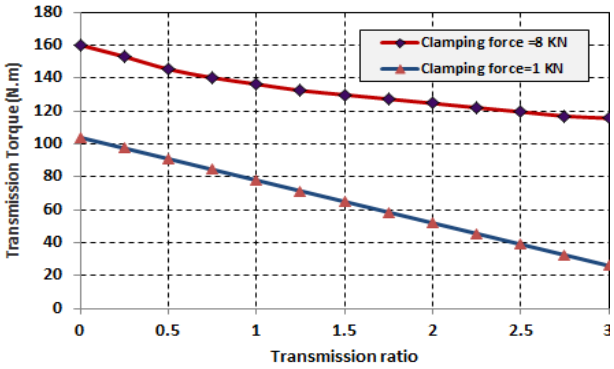

Fig. 10: Transmission torque vs. Transmission ratio

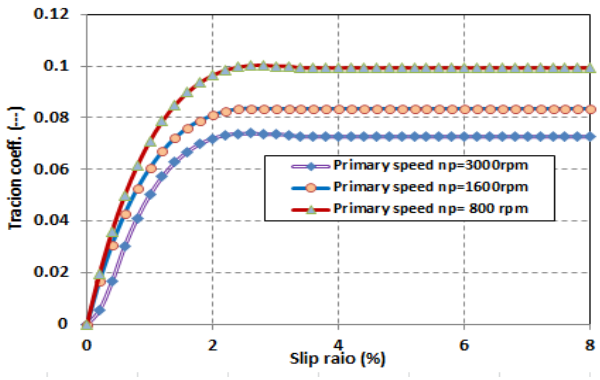

Fig. 11: Traction coefficient vs. Slip ratio for various speeds

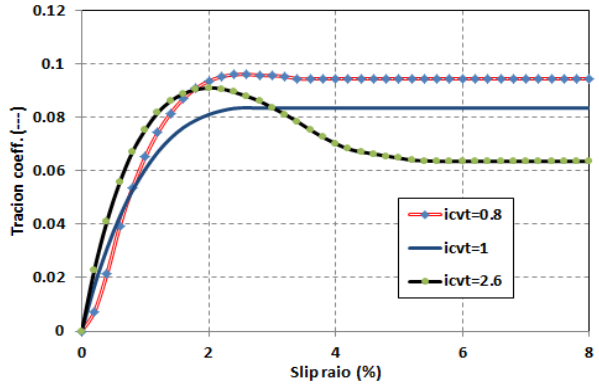

Fig. 12: Traction coeff. vs. Slip ratio for various reduction ratios

5. Experimental work

5.1. Test setup and measurements

Fig. 13 shows the test stand setup for measuring the performance of the push belt CVT. The experimental work consists of a 25 HP and 3000 rpm induction motor drawing power and driving a CVT belt system of Mitsubishi lancer GLX vehicle gearbox. A separate hydraulic brake is coupled to the output shaft of the CVT. The schematic diagram of the experimental set up with instrumentation details is shown in Fig. 14. The motor, hydraulic disc brake, CVT gearbox and hydraulic shift system are hard mounted and aligned on a bedplate. The bedplate is grounded using the isolation feet to prevent vibration transmission to the floor. The shafts are connected with both flexible and rigid couplings. The measurement uses an induction motor (1.5 HP and 1450 rpm) drawing power through an electrical source and driving hydraulic pump. The hydraulic shift system characteristics are listed in Table 2.

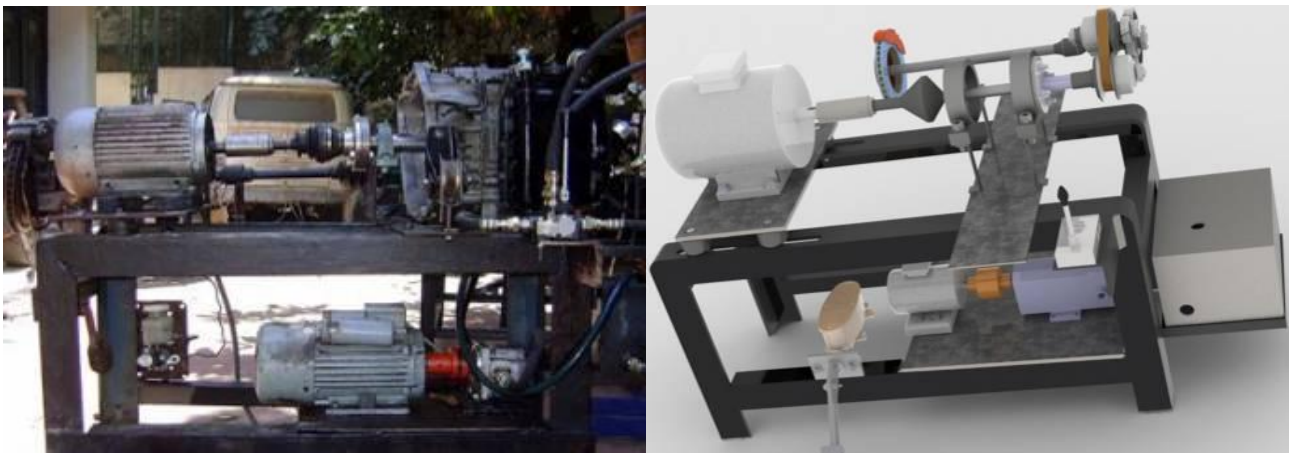

Fig. 13: Photographs of test rig and setup

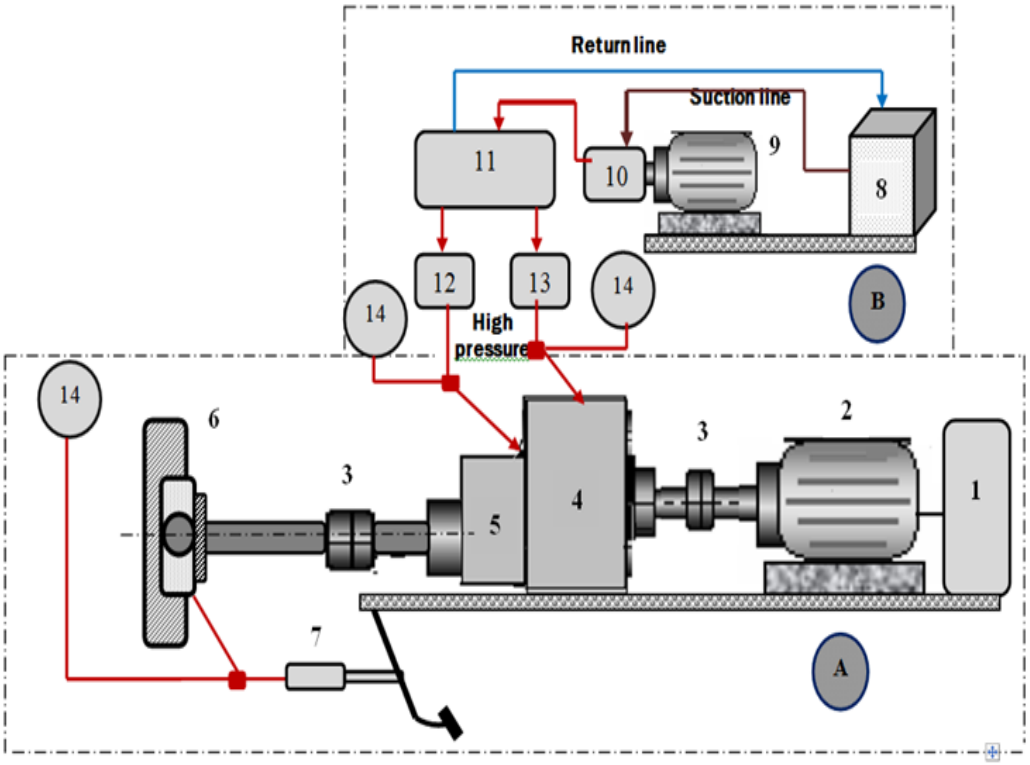

A	Mechanical Drive System	B	Hydraulic Drive System
1	3-phase inverter	8	Oil tank
2	Electrical drive motor	9	Electrical motor
3	Mechanical coupling	10	High pressure pump
4	Push belt CVT	11	Directional control valve
5	Differential final drive	12	Primary pulley choke valve
6	Brake system	13	secondary pulley choke valve
7	Brake master cylinder	14	Pressure gauge

Fig. 14: Schematic of test stand layout

Table 2: Hydraulic system characteristics

Parameter	Symbol	Unit	Value
Hydraulic pump flow rate	Q_p	*l*/min	10
Choke valve low rate	Q_c	*l*/min	15
DCV flow rate	Q_v	*l*/min	30
Oil tank capacity	V_{oil}	*l*	15
Secondary piston area	A_s	m^2	$10*10^{-3}$
Primary piston area	A_p	m^2	$20*10^{-3}$

The hydraulic part of the CVT consists of a gear pump directly connected to the driving electrical motor, the Directional Control Valve (DCV), choke valves and a pressure cylinder of the moveable pulley sheaves. The volume between the pump and the chock valves including the secondary pulley cylinder is referred to as the secondary circuit. The volume directly connected to the primary pulley cylinder is the primary circuit. Excessive flow in the secondary circuit bleeds off towards the accessories, whereas the primary circuit can blow off towards the drain. Pressures are defined relative to the atmospheric drain pressure p_T. The (DCV) directs the pressurized fluid to either primary or secondary pulley as set to position A or B as shown in Fig. 15. In neutral position the DCV returns the fluid to the tank. The Choke Valves (CV), the throttle choke valve allows the pressure flow normally in the forward direction and

restricts (choke) the flow in the return direction. It is used here to maintain the pressure level in the pulley after shifting the pressure direction to the other pulley.

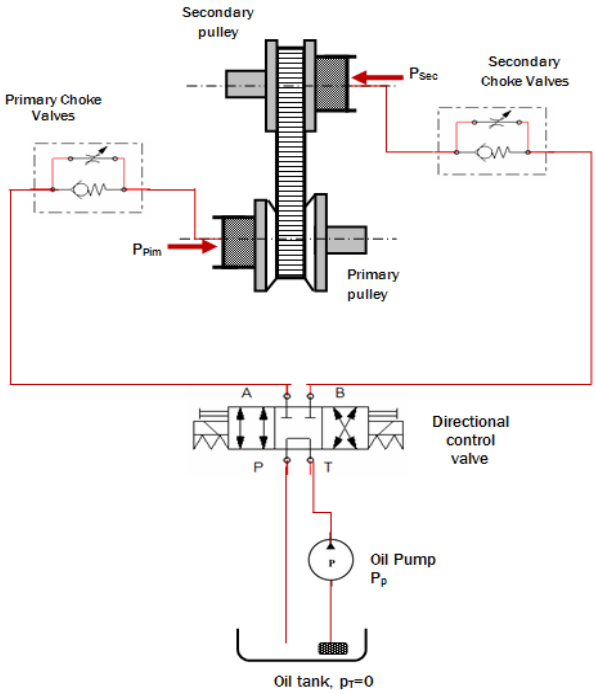

Fig. 15: Schematic diagram of hydraulic control circuit

As the model will only be used to determine the hydraulic system constraints needed for the feed forward control, the compressibility of the oil is neglected and the oil temperature is assumed as constant. All leakage flows are assumed as negligible. The clamping forces F_P and F_s are realized by the hydraulic cylinders on the moveable sheaves. Since these cylinders are at integrated with the pulleys, they rotate at very high speed. Hence centrifugal effects have to be taken into account and the pressure in the cylinders will not be homogeneous. Therefore, the clamping forces will also depend on the pulley speeds ω_{pri} and ω_{sec}. Furthermore, a pre-stressed linear elastic spring with stiffness K_s is attached to the moveable secondary sheave. This spring has to guarantee a minimal clamping force when the hydraulic system fails. Together this results in the following relations for the primary and secondary pulley clamping forces:

$$F_p = P_P * A_p + C_p * \omega^2{}_{pri} \tag{27}$$

$$F_S = P_s * A_s + C_s * \omega^2{}_{\sec} + K_s \Delta x + F_i \tag{28}$$

Here, A_p is the primary piston area. C_p is a centrifugal coefficient and P_p the oil pressure in the primary circuit. A_s is the secondary piston area. C_S is the centrifugal coefficient and P_s is the secondary pressure. Moreover, in F_s there is a contribution of the secondary spring F_{spr} that has to warrant a minimal clamping force under all circumstances. F_i is the force in the spring if the secondary moveable sheave is at position Δx=0.

The oil flow from the DCV to the primary circuit, by use the law of mass conservation, is applied to the primary circuit using,

$$Q_{DCV\to p} = C_f * A_p * x_p \sqrt{\frac{2(p_S - p_p)}{\rho} sign(p_s - p_p)} \tag{29}$$

Where C_f is a constant flow coefficient and ρ is the oil density. The equivalent valve opening area A_p depends on the primary valve stem position x_p. The oil flow from the primary circuit to the drain is given by,

$$Q_{p\to d} = C_f * A_{pd} * x_p \sqrt{\frac{2(p_p)}{\rho}} \tag{30}$$

Where A_{pd} is the equivalent opening area of the primary valve for the flow from primary circuit to the drain.

The oil flow from the DCV to the secondary circuit, by use of the law of mass conservation, is applied to the secondary circuit using,

$$Q_{DCV\to S} = C_f * A_p * x_s \sqrt{\frac{2(p_p - p_s)}{\rho} sign(p_p - p_s)} \tag{31}$$

The flow rate of oil pump is written as:

$$Q_{pump} = Q_{DCV\to S} + Q_{DCV\to p} + Q_{p\to d} \tag{32}$$

RMS of pressure and clamping force for discrete signals is defined as:

$$RMS = \sqrt{\frac{1}{N}\sum_{n-1}^{N}\left(x(n) - \bar{x}\right)^2} \tag{34}$$

Where N is the number of samples taken within the signal and $x(n)$ the time domain signal. $\bar{x}$ is the mean value of all the amplitudes as given by,

$$\bar{x} = \frac{1}{N}\sum_{n=1}^{N} x(n) \tag{35}$$

5.2. Test results and discussions

A National Instruments LabVIEW program version 7.1 was used to create the desire software program to perform the required laboratory tests. The speed variation can be accomplished by varying the frequency to the motor with an AC inverter unit. The motor shaft speed is varied from 800 rpm to 3000 rpm. The load variation values by hydraulic brake system is from 0 to 75 Nm. Fig. 16 and Fig. 17 show the translation primary and secondary pressure responses in time-domain, for input speed of 800 and 2400 rpm respectively. The maximum oil pressure acting on secondary pulley piston is 48 bars at input speed 800 rpm and decrease to 45 bars at increased input speed of 3000 rpm. Fig. 18 and Fig. 19 show the translation primary and secondary clamping responses in time-domain.

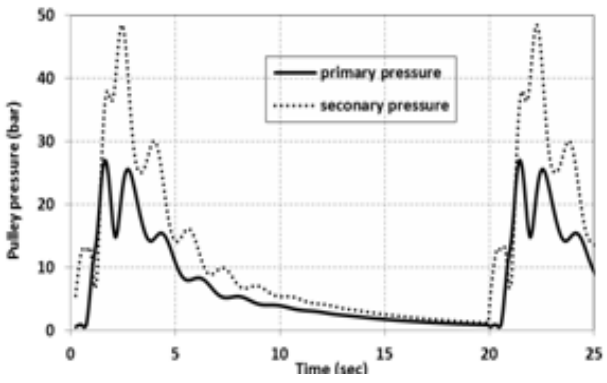

Fig. 16: Primary and secondary pressure responses at 800 rpm

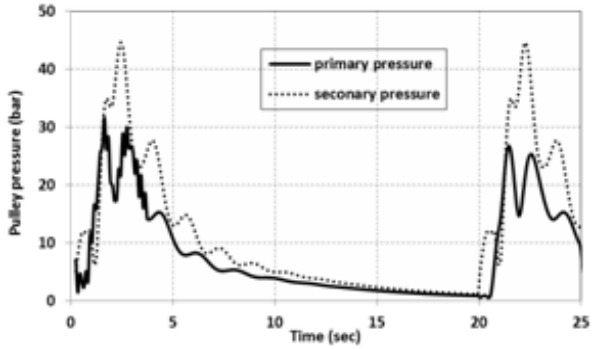

Fig. 17: Primary and secondary pressure responses at 3000 rpm

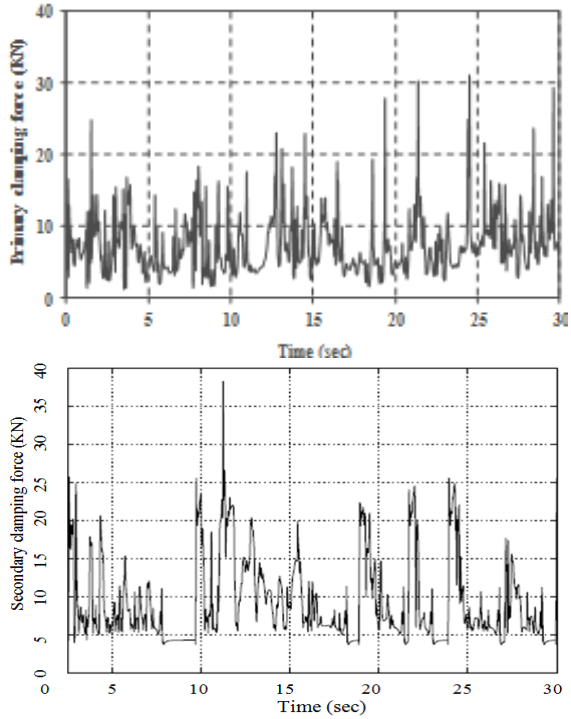

Fig. 18: Primary & secondary clamping force responses at 800 rpm

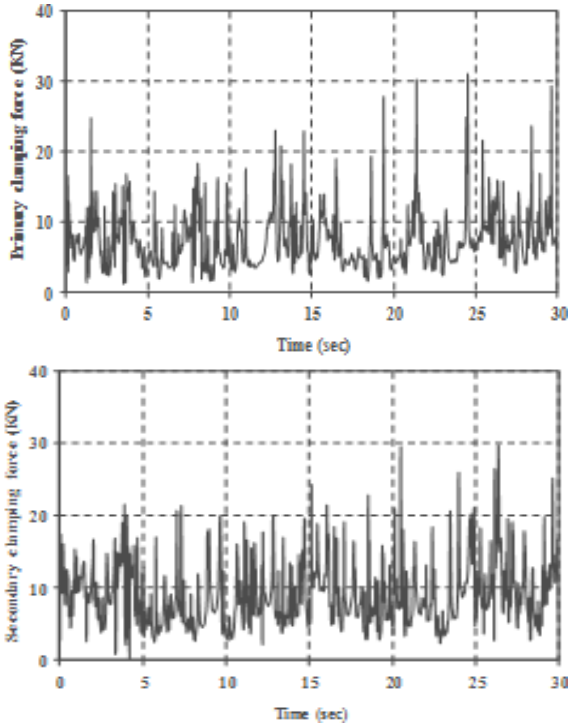

Fig. 19: Primary & secondary clamp. force responses at 3000 rpm

5.3. Comparison of simulation and test results

Simulation and experimental results at 1600 rpm are compared. Fig. 20 shows the traction coefficient at different transmission ratio and the measured clamping force effects on the fluctuations of the traction coefficient. Fig. 21 illustrates the transmission efficiency at i_{cvt}=2.6.The maximum value of efficiency is 94% from simulation and 90 ± 2% from experiment. The transmission efficiency depends on oil pressure, transmission ratio and input speed. Fig. 22 and Fig. 23 illustrate the RMS of clamping force for different output load, speed and i_{cvt}=2.6. Fig. 24 illustrates the maximum value of transmission efficiency for different clamping force. The transmission efficient of the CVT increases for a decrease in the clamping force and the transmission ratio is kept constant.

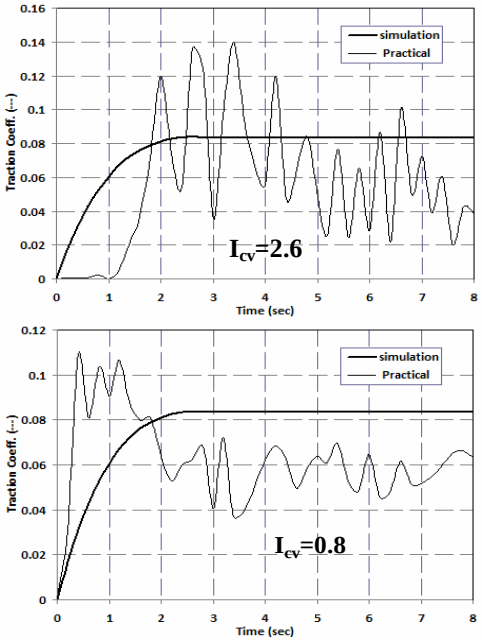

Fig. 20: Comparison between simulation and test traction coefficient at 1600 rpm

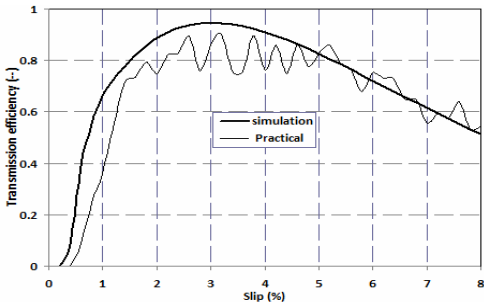

Fig. 21: Simulation vs. Test: Transmission efficiency at 1600 rpm

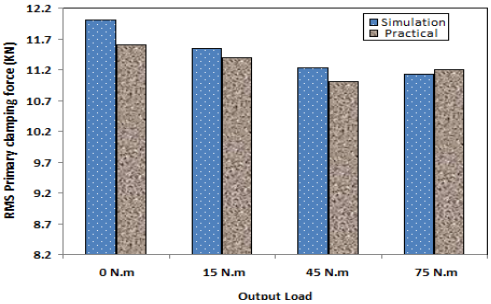

Fig. 22: Simulation vs. Test: RMS of clamping force at 1600 rpm

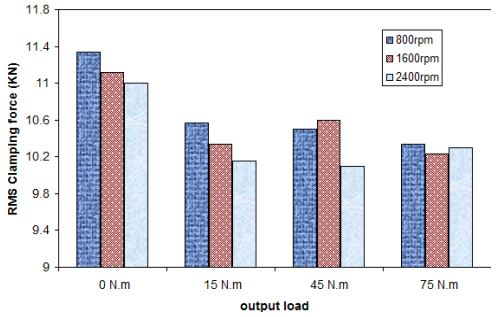

Fig. 23: Test RMS of clamping force for different input speed

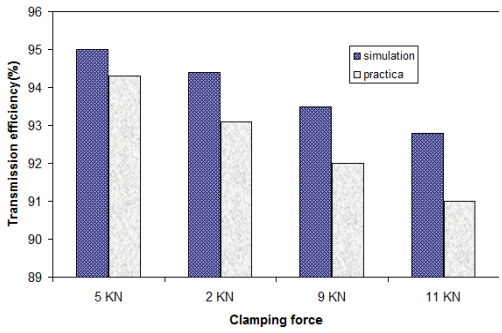

Fig. 24: Simulation vs. Test: Transmission efficiency for different clamping force

6. Conclusions

In this paper, the dynamic analysis and experimental work with artificial clamping force of metal V- type push belt of CVT was presented. Applying the different input variable parameters to the push belt system mathematical model, the input speed (ω_P), the transmission ratio (i_{cvt}), the half pulley wedge angle (θ), and the slip ratio, directly affects the system transmission performance. Based on the RMS of applied pressure and clamping force of CVT gearbox, the influence of changing gearbox speed and load on the RMS value is also discussed. The laboratory test rig and experimental methodology capability established in this work could be utilized for evaluating the dynamic performance of the push belt CVT. Theoretical and experimental comparison of a belt drive variation in steady state conditions have shown a good agreement between simulation and experiments especially at high clamping forces values, either to predict the thrust force ratio necessary to establish the desired transmission ratio or to evaluate the variator traction behaviour.

REFERENCES:

[1] S. Kuwabara, T. Fujii and S. Kanehara. 1999. Study on a metal pushing V-belt type CVT: band tension and load distribution in steel rings, *J. SAE review*, 20, 55-60. http://dx.doi.org/10.1016/S0389-4304(98)00040-X.

[2] H. Kim and J. Lee. 1994. Analysis of belt behaviour and Slip Characteristics for a metal V-belt CVT, *Mechanism & Machine Theory*, 29(6), 865-876. http://dx.doi.org/ 10.1016/0094-114X(94)90086-8.

[3] V.D. Browne. 1996. Metal belt CVT's - Torque capacity, *ASME Proc. Int. Power Transmission and Gearing Conf.*, 7, 453-457.

[4] M. Gangadurl, N. Harikrishnan and B. Sreekumar. 2005. Development of an analytical design concept of mechanical controlled continuously variable transmission, *SAE Paper 2005-26-069*.

[5] H. Shimizu, D. Kobayashi, J. Kawashima and Y. Kato. 2000. Development of 3-D simulation for analyzing the dynamic behaviour of a metal pushing V-belt for CVTs, *SAE Paper 2000-01-0828*.

[6] M.P. Bas, V.S. Bart, V. Frans and S. Maarten. 2006. Control of a hydraulically actuated continuously variable transmission, *Vehicle System Dynamics*, 44(5), 387-406. http://dx.doi.org/10.1080/00423110500244088.

[7] G. Carbone, L. Mangialardi and G. Mantriota. 2002. Influence of clearance between plates in metal pushing V-belt dynamics, *ASME J. Mech. Design*, 124, 543-557. http://dx.doi.org/10.1115/1.1486015.

[8] N. Srivastava. 2006. *Modeling and Simulation of Friction Limited Continuously Transmission*, PhD Thesis, Dept. of Mech. Engg., Clemson University, USA.

[9] S. Bdran, M. Shuyuan, S. Saifullah and J. Huang. 2013. Control speed ratio electro-hydraulic system of continuously variable transmission by robust PI controller, *IACSIT Int. J. Engineering and Technology*, 5(5), 561-565. http://dx.doi.org/10.7763/IJET.2013.V5.618.

[10] E.S. Mohamed. 2013. Design and performance analysis of the hybrid powertrain strategies for split hybrid vehicles with CVT, *Int. J. Electric and Hybrid Vehicles*, 5(3),195-214. http://dx.doi.org/10.1504/IJEHV.2013.057605.

[11] B. Pennings, D. Mark van, B. Arjen, G. Erik van and L. Marlène. 2003. Van Doorne CVT fluid test: A test method on belt-pulley level to select fluids for push belt CVT applications, *SAE Paper 2003-01-3253*.

[12] C.R. Willis. 2006. *A Kinematic Analysis and Design of a Continuously Variable Transmission*, MSc Thesis, Dept of Mech. Engg., Virginia Polytechnic Institute and State University, USA.

[13] B. Bonsen. 2006. *Efficiency Optimization of the Push-belt CVT by Variator Slip Control*, PhD Thesis, Technische Universiteit Eindhoven, Netherlands.

[14] Z. Lu. 1998. *Acceleration Simulation of a Vehicle with a Continuously Variable Power Split Transmission*, MSc Thesis, Dept. of Mech. Engg., West Virginia University, USA.